Proceedings of the ASME 2009 International Mechanical Engineering Congress & Exposition
IMECE2009
November 13-19, Lake Buena Vista, Florida, USA

IMECE2009-13007

CONTROL OF A ROBOTIC UV CURING PROCESS WITH THERMAL VISION FEEDBACK THROUGH TWO IR CAMERAS

Fan Zeng, Beshah Ayalew, and Mohammed Omar
International Center for Automotive Research
Clemson University, Clemson, SC, USA

ABSTRACT

Robotic ultra-violet (UV) curing is considered to be one of the effective ways to replace the current convection-based methods in various manufacturing processes due to its fast curing rate and high energy efficiency. This paper presents a closed-loop control of a robotic UV curing system by using thermal vision feedback through two infrared (IR) cameras. The proposed approach is developed based on a mathematical analysis of the fundamental UV curing process and the integration of the local and global IR cameras in a cascade manner. A computer simulation study is conducted to evaluate the proposed strategy by regarding two control variables: the radiant intensity of the UV heater and the sweeping speed of the robot end effector. The results indicate that controllers using either control variable can compensate for interferences and improve curing quality under this thermal-vision-based architecture.

KEYWORDS

Robotic curing, UV curing, Thermal signature feedback, Local and global camera, Cascade control

INTRODUCTION

Ultraviolet (UV) curing is radiation-based hardening technology typically used in temperature-sensitive coating, printing and adhering processes [1]. Due to its high energy efficiency and short processing time, this technology is now expanding to a large area of new applications (e.g. automotive exterior paint curing) in which the curing is traditionally done by other methods, such as convectional baking. However, most of these new applications which use fixed UV sources face great challenges in achieving uniform curing quality due to the limitation of the UV sources and complexity of the target surface. To improve the flexibility, industrial manipulators can be used to perform the curing task by carrying the UV heater and sweeping the target surface in a pre-designed trajectory [2, 3].

Generally, the quality of the above robotic UV curing process is ensured by repetitive trial tests in which the curing parameters are calibrated and then used to optimize the trajectory of the manipulator. Sometimes, this open-loop mechanism may not work when interferences occur during the curing process. In addition, the change of curing target usually requires further repetitions of the calibration process and increases the total time and cost. To improve the performance of the robotic UV curing, the authors proposed some closed-loop control methods employing online thermal vision feedback [4, 5]. These methods involve using an infrared (IR) camera to monitor the temperature of the target surface and mapping it to the conversion of curing. The measured curing status is then incorporated in the control the UV source in real time.

In this paper, the thermal-vision-based approach is enhanced to control the robotic UV curing process by using two IR cameras, one of which is mounted on the end effector of the robot manipulator and the other is fixed to the curing cell. In this approach, the thermal vision from the two cameras is integrated into a cascade controller to achieve closed-loop control of the curing process. Simulation is conducted to evaluate the proposed approach.

The rest of this paper is organized as follows. The next section states the basic control problem for robotic UV curing. This is followed by the section that details the proposed control approach based on thermal vision feedback through two IR cameras. Then the corresponding process simulation results are presented. Finally, the last section summarizes the conclusions of this work and addresses future effort.

PROBLEM DESCRIPTION

A. Fundamentals of the UV Curing

In general, the UV curing process is composed of three essential parts: irradiation, photo-initiated polymerization and thermal evolution [1, 6]. The individual contribution of each part to the curing process can be described by the energy balance equation below [6, 7].

$$\rho_p \cdot c_p \cdot \frac{dT_p}{dt} = \nabla\left(\lambda_p \nabla T_p\right) - \Delta H \cdot R_p + \varepsilon[\mathrm{PI}]I \qquad (1)$$

Here, the left-hand side of equation (1) indicates the energy change with respect to time which is described by density (ρ_p), specific heat capacity (c_p) and the temperature (T_p) derivative at the current coordinate. The right-hand side describes the energy input and output, including the heat transfer by conduction, heat generation by the polymerization reaction, and the absorption of the UV irradiation. λ_p denotes the thermal conductivity of the paint film. ΔH and R_p represent the polymerization enthalpy and reaction rate. The last term of the right-hand side is described by the extinction coefficient (ε), the concentration of the photo-initiator ($[\mathrm{PI}]$) and the UV irradiance (I) at the current coordinate. Given the above equation, the main energy contribution is determined by the reaction rate (R_p) and UV irradiance (I) once other parameters associated with paint and polymerization have been selected. The correlation between R_p and I can be characterized by [6]:

$$R_p = \frac{k_p}{k_t^{0.5}} \cdot [\mathrm{M}] \cdot \left(\phi \cdot \varepsilon[\mathrm{PI}]I\right)^{0.5} \qquad (2)$$

where k_p, k_t represent the rate constant of propagation and termination respectively, $[\mathrm{M}]$ is the monomer concentration, and ϕ denotes the quantum yield of initiation. Both equation (1) and (2) indicate that the UV irradiance I plays such a significant part in energy exchange of the whole curing process that achieving the proper irradiance distribution (temporal and spatial) should be considered as the primary goal of the control design effort.

B. Control Problem Description

Given the fundamentals of UV curing mentioned above, the main objective of the robotic curing is to achieve a proper distribution of the UV irradiance on the target surface by controlling the UV heater and motion of the manipulator. Considering a basic robotic UV curing task illustrated in Fig-1, the target is located in the global frame while the manipulator holds the UV heater (an LED type is used here) and sweeps the target surface in a specific trajectory which can be either designed in advance or generated online. The LED frame is assumed to be identical with the local frame of the end effector.

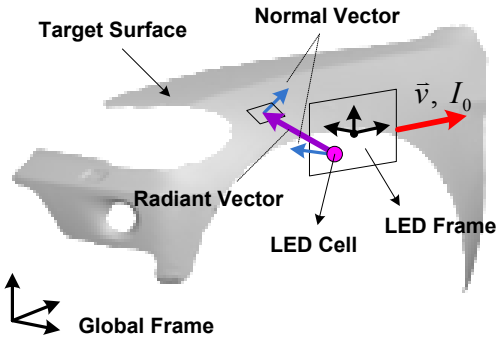

Fig-1 A basic robotic UV curing task

Here, $\vec{v}$ and I_0 denote the speed of the end effector and the intensity of the UV LED. In the following parts, the suitable relationship between the irradiance distribution on the target surface and the motion of the manipulator is derived.

Generally, the UV irradiance I ($\mathrm{w/m^2}$) is defined as the power of UV light reaching at each unit area of the target surface. The distribution of irradiance is determined by the radiant characteristics of the UV source and current location of the end effector. The calculation of irradiance at any unit area of the surface can be depicted in Fig-2.

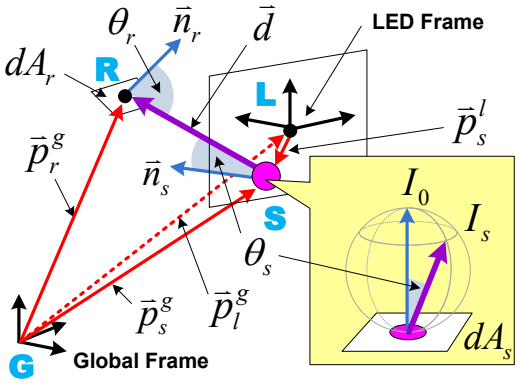

Fig-2 The calculation of the irradiance

Here, G and L denote the origins of the global and LED frames, respectively. S and R represent a single cell of the UV LED and a unit area of the target surface. Then, the irradiance calculation can be performed in an inverse order.

1) Present the expression of irradiance at the unit R

According to the fundamental radiation theory [8, 9], the irradiance at the unit R showed in Fig-2 can be described by:

$$I = k \cdot \frac{I_s \cos\theta_r}{\left|\vec{d}\right|^2} \qquad (3)$$

where k is an efficiency factor describing the absorption characteristics of the target surface. I_s is the incident radiant

intensity defined as the power per solid angle (W/sr). θ_r denotes the angle of the incident direction and the normal direction of the unit R. $\vec{d}$ represents the vector from the UV cell S to the unit R and $|\vec{d}|$ is the associated relative distance.

2a) Calculate the incident radiant intensity

The incident radiant intensity (I_s) in equation (3) is determined by the characteristics of the UV LED which can be simply modeled by a superposition of several Lambertian point sources. The radiant intensity distribution of a single Lambertian source is described by [8]:

$$I_s = I_0 \cdot \cos\theta_r \tag{4}$$

In equation (4), I_0 is the radiant intensity along the normal direction of the cell which also determines the radiant capability of the UV source. θ_r represents the angle between the radiant and normal directions. It is apparent that the maximum intensity is always found in the normal direction of the UV cell and it is also one of the most important factors which can influence the irradiance distribution on the target surface.

2b) Calculate the relative configuration between S and R

According to equation (3), another key factor which determines the irradiance is the relative configuration between the UV cell S and the unit R. This can be characterized by the vector $\vec{d}$, the radiant angle θ_s, and the incident angle θ_r. Considering the global frame shown in Fig-2, the vector $\vec{d}$ can be calculated by:

$$\vec{d} = \vec{p}_r^{\,g} - \vec{p}_s^{\,g} \tag{5}$$

where $\vec{p}_r^{\,g}$, $\vec{p}_s^{\,g}$ represent the vector from G to R and the one from G to S in the global frame. Since the target is fixed to the global frame, the vector $\vec{p}_r^{\,g}$ is time invariant. On the other hand, the vector $\vec{p}_s^{\,g}$ will change with respect to time due to the motion of the end effector. According to Fig-2, the point S (cell) can also be represented in the LED frame by using the vector $\vec{p}_s^{\,l}$ from L to S. Then, the vector $\vec{p}_s^{\,g}$ can be calculated by $\vec{p}_s^{\,l}$ through homogeneous transformation [10].

$$\vec{p}_s^{\,g} = \left({}^{g}K_l\right)^{-1} \vec{p}_s^{\,l} \tag{6}$$

The matrix ${}^{g}K_l$ represent the homogeneous transformation from the global frame to the LED frame which can be obtained by calculating the direct kinematics of the manipulator [10, 11]. Substituting equation (6) into (5) yields:

$$\vec{d} = \vec{p}_r^{\,g} - \left({}^{g}K_l\right)^{-1} \vec{p}_s^{\,l} \tag{7}$$

Considering the right-hand side of equation (7), only the term ${}^{g}K_l$ will vary with the motion of the end effector and it is determined by all the joint angles of the manipulator. Other aspects of the relative configuration are two important angles: θ_s and θ_r, which can be calculated by:

$$\cos\theta_s = \frac{\vec{d} \bullet \vec{n}_s}{|\vec{d}||\vec{n}_s|} = \frac{\vec{d} \bullet \vec{n}_s}{|\vec{d}| \cdot 1} = \frac{\vec{d} \bullet \vec{n}_s}{|\vec{d}|} \tag{8}$$

$$\cos\theta_r = \frac{\vec{d} \bullet \vec{n}_r}{|\vec{d}||\vec{n}_r|} = \frac{\vec{d} \bullet \vec{n}_r}{|\vec{d}|} \tag{9}$$

Here, $\vec{n}_s$ and $\vec{n}_r$ are normal vectors of the cell S and unit R from the view of the global frame.

Combing 2a) and 2b) gives the overall calculation of irradiation based on the radiant intensity and relative geometric configuration.

$$I = k \cdot \frac{I_0 \cos\theta_s \cos\theta_r}{|\vec{d}|^2} = k \cdot \frac{I_0 (\vec{d} \bullet \vec{n}_s) \cdot (\vec{d} \bullet \vec{n}_r)}{|\vec{d}|^4} \tag{10}$$

$$\vec{d} = \vec{p}_r^{\,g} - \left({}^{g}K_l\right)^{-1} \vec{p}_s^{\,l} \tag{11}$$

The above two equations describe the contribution of a single cell (S) of the UV LED to the irradiance of a unit R on the target surface. Then the total irradiance at R can be obtained through superposition. Now, recalling equation (1), the final control problem can be simply described by:

$$\frac{dT_p}{dt} = f\left(T_p\right) + g\left(I_0\ ,\ {}^{g}K_l\right) \tag{12}$$

where T_p represents the temperature of any unit of the target surface which varies with time and coordinate. f denotes the function describing the heat transfer characteristics. The function g integrates the irradiation and polymerization processes which are mainly influenced by the radiant intensity I_0 and relative geometric configuration ${}^{g}K_l$.

THERMAL-VISION-BASED CONTROL

Given the system dynamics described in equation (12), the open-loop control of the robotic curing process is achieved by imposing a calibrated radiant intensity and relative geometric configuration. However, such open-loop control is not robust enough to compensate for interferences, like uneven paint or geometric jump in a practical curing task. If some kind of feedback regarding the curing status is introduced, then the control input can be adjusted online and the corresponding curing quality will be greatly improved.

In this section, a closed-loop control approach will be discussed, in which the feedback is provided by two IR cameras

monitoring the temperature of the target surface (thermal vision). The following paragraphs will describe the details of the proposed method.

A. Basic Control Architecture

The proposed closed-loop control approach is designed in a cascade manner which incorporates both the motion and thermal vision feedback. The basic control architecture is illustrated in Fig-3.

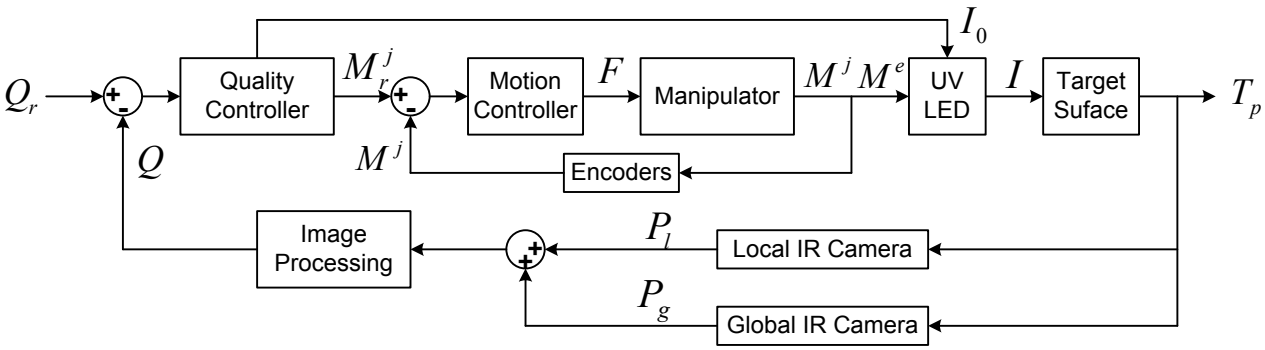

Fig-3 The basic architecture of the proposed control approach

The control system in Fig-3 is composed by two closed loops. The inner loop is the motion control which regulates the manipulator's motion according to the reference trajectory generated by the upper controller. M_r^j, M^j represent the reference and actual motion of the joints, and M^e denotes the actual motion of the end effector. F is the torque applied to each joint. The outer loop is the curing quality control which acquires the online curing status through two IR cameras and generates the reference (motion and radiant intensity) for the manipulator and UV LED. Here, Q_r, Q represent the reference and actual curing quality. I_0, I denote the normal radiant intensity of the UV LED and the actual irradiance distribution on the target surface. P_l, P_g represent the thermal images obtained by the two IR cameras. T_p is the temperature distribution of the target surface.

B. Implementation of the Thermal Vision Feedback

In the proposed control approach, the thermal vision feedback is provided by two IR cameras, one of which ("Local") is installed on the end effector of the manipulator and the other ("Global") is fixed to the global frame. Generally, the local camera can monitor the current under-cured area in real time since it is moving with the UV LED and close to the target surface. On the other hand, the global camera can acquire information from other areas, especially those which have been cured, and give the estimation of curing quality. The individual application of each IR camera in the control of the robotic UV curing process has been discussed by the authors in [5]. Now, a new implementation which combines both of the two IR cameras will be presented.

The general monitored variable for the local and global IR cameras is the temperature distribution of the target surface. In this paper, it is simply assumed to be equivalent to the distribution of conversion of curing (In practice, the exact correlation between the two can be obtained through calibration). Fig-4 shows an illustration of such a distribution on a rectangular area during the curing process.

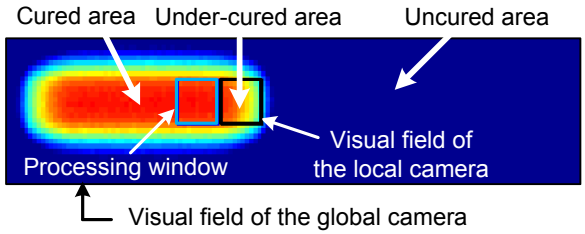

Fig-4 A sample of the temperature distribution

The temperature distribution showed in Fig-4 indicates the current position of the end effector and UV LED, which is around the center of the under-cured area. The black window represents the visual field of the local IR camera, including most of the under-cured area. The outside of the black window is monitored by the global camera. A processing window is used to estimate the quality of the just cured area.

Once the local and global thermal images have been acquired by the two IR cameras, some statistic features can be extracted to estimate the curing quality. Considering the two windows in Fig-4, the average temperature of each is defined below.

$$\bar{T}_p^l = \frac{1}{N_l}\sum_{i=1}^{N_l} T_{pi}^l \qquad (13)$$

$$\bar{T}_p^g = \frac{1}{N_g}\sum_{i=1}^{N_g} T_{pi}^g \tag{14}$$

where T_{pi}^l, T_{pi}^g represent the temperature at each pixel within the local and global processing windows. N_l and N_g denote the number of pixels for each window. In addition, to describe the transition characteristics within the local processing window, a cured / uncured temperature ratio is given by:

$$h = \frac{\bar{T}_{pc}^l}{\bar{T}_{pu}^l} = \frac{(1/N_{lc})\cdot\sum_{i=1}^{N_{lc}}\left(T_{pi}^l \,|\, T_{pi}^l \geq T_0\right)}{(1/N_{lu})\cdot\sum_{i=1}^{N_{lu}}\left(T_{pi}^l \,|\, T_{pi}^l < T_0\right)} \tag{15}$$

Here, $\bar{T}_{pc}^l$ and $\bar{T}_{pu}^l$ represent the average temperature of the cured and uncured part of the local processing window. T_0 is the temperature threshold. N_{lc}, N_{lu} denote the number of pixels at which the temperature is above and below the threshold T_0.

Given their own definitions above, $\bar{T}_p^l$ and $\bar{T}_p^g$ can be used to estimate the conversion of curing for the under-cured and cured areas. The temperature ratio h can help detect the occurrence of the interferences. Based on the three statistic features extracted from the thermal images, the quality controller is designed as:

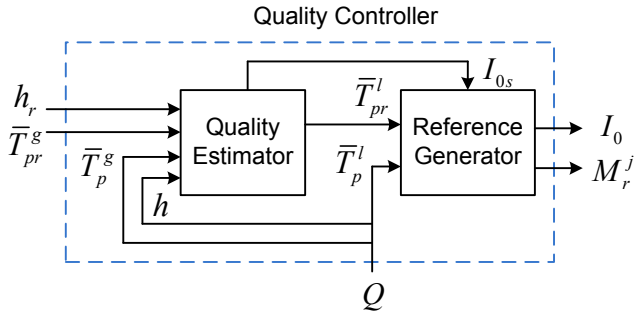

Fig-5 Quality controller design

In Fig-5, the quality estimator calculates the local quality reference $\bar{T}_{pr}^l$ for the reference generator based on the desired curing quality (h_r, $\bar{T}_{pr}^g$) and the measured curing status (h, $\bar{T}_p^g$). It also controls the shift radiant intensity I_{0s} of the UV LED (discussed later). Then the reference generator calculates the reference motion (M_r^j) of the manipulator and radiant intensity I_0 by comparing the desired and actual local quality ($\bar{T}_{pr}^l$, $\bar{T}_p^l$). This hybrid structure not only ensures the overall curing quality but also has the ability for interference compensation due to the thermal vision feedback from both the local shot and the global picture.

C. *Motion Control Design*

The motion of the manipulator is controlled in the joint space by using the joint position and velocity feedback through encoders. An inverse dynamic algorithm can be used to generate the control torques [4, 5]. In this algorithm, the reference trajectories including the position, velocity and acceleration of each joint are pre-designed through inverse kinematics but can also be adjusted by the quality controller in real time.

SIMULATION RESULTS

In this section, an example case will be studied by simulation to evaluate the proposed approach. The platform includes a PUMA560 robot model established in the multi-body software SIMPACK, a basic curing model developed in Matlab/Simulink, and a co-simulation mechanism between the two software environments. The control strategy is also developed in Matlab/Simulink and is implemented to cure a simple rectangular target which is depicted in Fig-6.

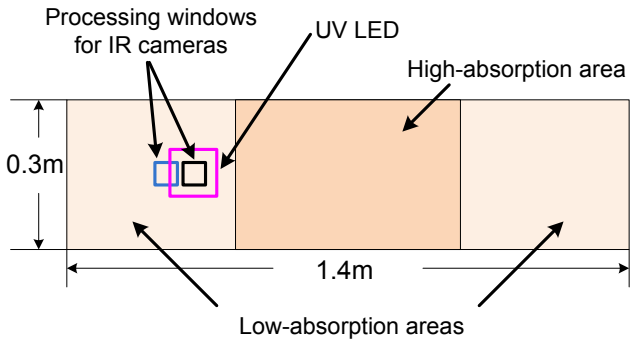

Fig-6 The rectangular target for curing

In Fig-6, the rectangular target has a dimension of 1.4×0.3m and it is also modeled by a 140×30 cell matrix in Matlab. The target surface is divided into three parts: the middle part has a high absorption of UV light and the sides are low-absorption areas. The difference in absorption can be used to describe the interference during the curing process. It is obvious that a simple open-loop sweep on this surface will cause uneven curing. The proposed closed-loop control approach through IR cameras is implemented to this target and the corresponding results will be discussed in the following paragraphs.

The curing model in this simulation is simply described by two parts: the radiation of the UV LED and the energy accumulation at the target surface. The transition stages caused by polymerization and heat conduction are ignored here. The UV LED appearing in Fig-6 is model by a 10×10 matrix (0.1×0.1m), each element of which can be considered as a Lambertian source described in equation (4). The energy accumulation at the target surface can be calculated by:

$$E(dA_r,t)=\int_0^t dt\cdot\int_{As} k\cdot\frac{I_0\cos\theta_s\cos\theta_r}{\left|\vec{d}\right|^2}\cdot dA_s \qquad (16)$$

If the energy required for a full cure on each unit of the target surface is set to E_0, then the normalized energy accumulation or the conversion of curing can be defined by:

$$x_c = E(dA_r,t)/E_0 \qquad (17)$$

Since the transition effect is ignored, the energy accumulation at the target surface is assumed to be equivalent to the temperature. Then the conversion of curing is also represented as:

$$x_c = T_p(dA_r,t)/T_c \qquad (18)$$

Here, $T_p(dA_r,t)$ is the current temperature at each unit of the target surface and T_c is a constant temperature at which the unit has been completely cured. Given the correlation between temperature and energy accumulation, we can use the normalized energy accumulation or conversion of curing x_c to replace the temperature $T_p(dA_r,t)$ as the feedback variable from the IR camera. The processing windows for the local and global cameras have been shown in Fig-6. Each of them is modeled by a 5×5 matrix in Matlab.

The implementation of the proposed control strategy is done in two different cases. Either the radiant intensity I_0 or the relative geometric configuration ${}^gK_l$ can be controlled by using the thermal vision feedback through the local and global IR cameras. Their influence on the curing quality is discussed below.

A. Radiant Intensity Control

The radiant intensity control is applied based on the condition that the relative geometric configuration between the UV LED and target surface is fixed, which means the distance between UV LED and target surface, the sweeping speed, and the orientation of the end effector are kept constant during the curing process. In this case, the distance and sweeping speed are selected as 0.025m and 0.3 m/s. The UV LED is oriented perpendicular to the target surface by the end effector and the initial radiant intensity is set as 36 W/sr. The desired conversion of curing is set as 0.8.

Now the task is to control the radiant intensity of the UV LED by using the proposed strategy so that the desired curing quality can be achieved. First, the open-loop sweep with the above parameters will be performed to generate a baseline curing. The corresponding results are shown in Fig-7 ~ 9.

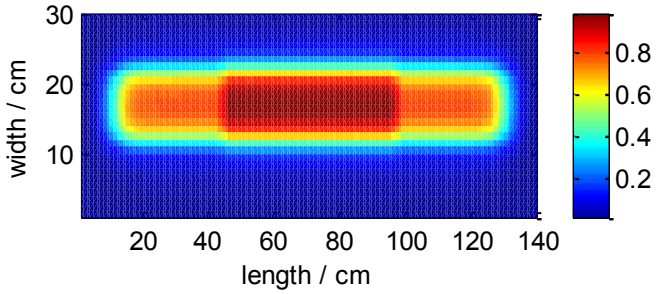

Fig-7 The conversion of curing through the target surface

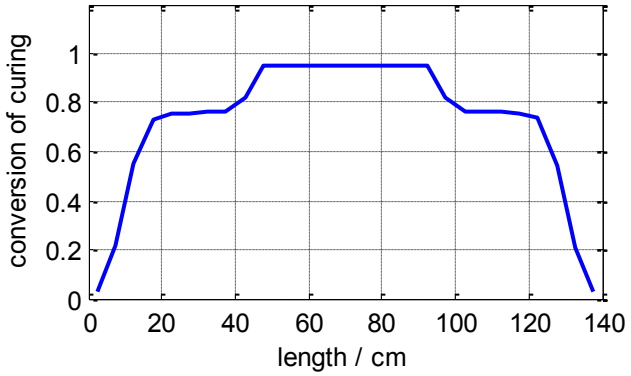

Fig-8 The conversion of curing along the centerline

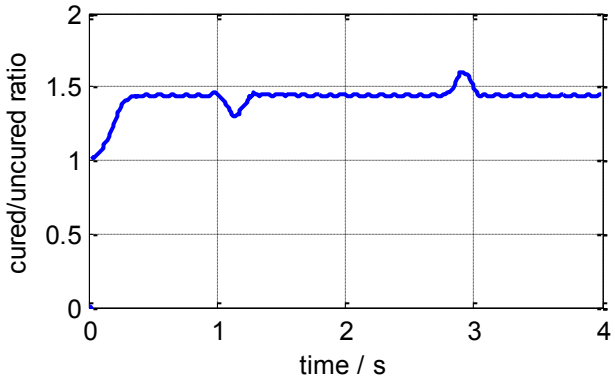

Fig-9 The time history of the cured / uncured ratio

The unevenness illustrated in both Fig-7 and 8 indicates that the open-loop sweep fails to compensate for the interference described in Fig-6. Fig-9 depicts the time history of the cured / uncured ratio h which shows the occurrence of the interference as observed by the local camera. By using the thermal vision feedback, the radiant intensity can be adjusted during the curing process and the above interference will be counteracted. The corresponding control structure is illustrated in Fig-10.

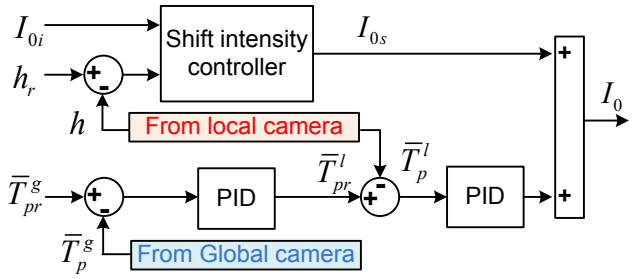

Fig-10 The radiant intensity controller

In Fig-10, the global camera monitors the average temperature $\bar{T}_p^g$ (equivalent to conversion of curing) of the cured area within the processing window. It is compared with the global reference $\bar{T}_{pr}^g$ and then a PID controller is applied to generate the local reference $\bar{T}_{pr}^l$. This will be compared with the local average temperature $\bar{T}_p^l$ monitored by the local camera and another PID controller is used to calculate the radiant intensity. A shift intensity I_{0s} is introduced and controlled under the strategy that I_{0s} is reduced (increased) after a negative (positive) deviation of h from h_r and the change of intensity is proportional to the deviation. The corresponding results are shown in Fig-11 ~ 13.

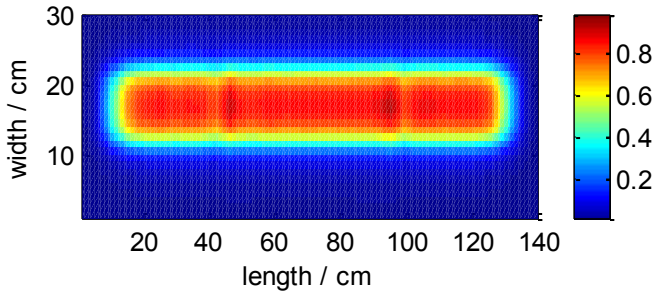

Fig-11 The conversion of curing through the target surface by radiant intensity control

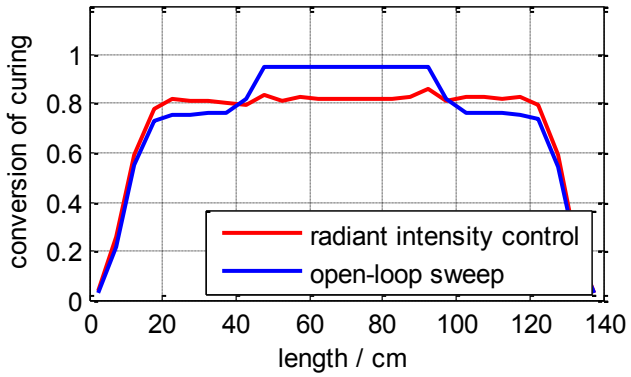

Fig-12 The conversion of curing along the centerline for two curing methods (radiant intensity control, open-loop sweep)

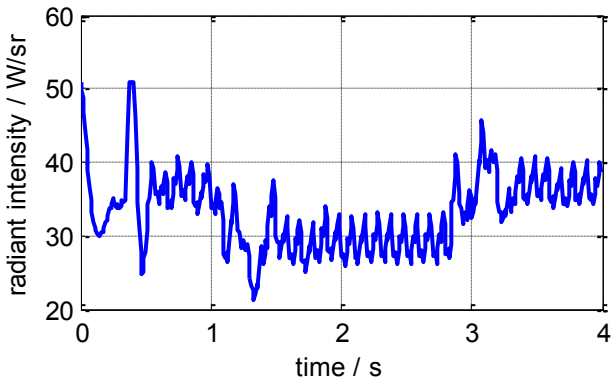

Fig-13 The time history of the radiant intensity

It can be seen from Fig-11 and 12 that the curing uniformity is greatly improved by controlling the radiant intensity through thermal vision feedback. The reason why the interference has been overcome can be explained by Fig-13, in which the average radiant intensity is reduced when the end effector crosses the middle area which has a higher absorption of UV radiation than the sides.

B. Relative Geometric Configuration Control

In this case, the radiant intensity remains constant and the relative geometric configuration between the UV LED and the target surface is controlled through thermal vision feedback. Here, only control of the speed of the end effector is considered and the other two parameters (distance, orientation) are fixed. The structure of the speed control is represented by:

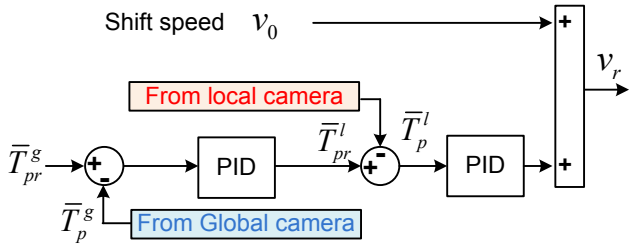

Fig-14 The speed controller

Similar to above, the first PID controller is used to generate the local reference $\bar{T}_{pr}^l$ by comparing the global feedback $\bar{T}_p^g$ with the desired curing quality $\bar{T}_{pr}^g$. The task of the second PID controller is to regulate the local curing status $\bar{T}_p^l$ by adjusting the speed of the end effector. A constant shift speed v_0 is used to initialize the motion of the end effector. The associated results are illustrated in Fig-15 ~ 17.

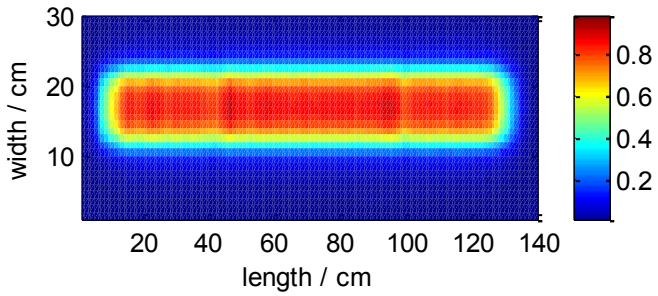

Fig-15 The conversion of curing through the target surface by speed control

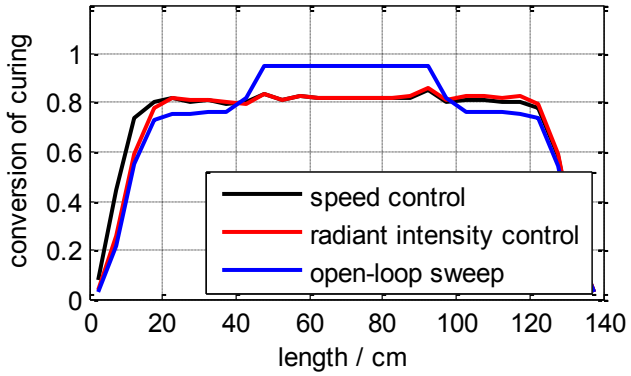

Fig-16 The conversion of curing along the centerline for the three curing methods

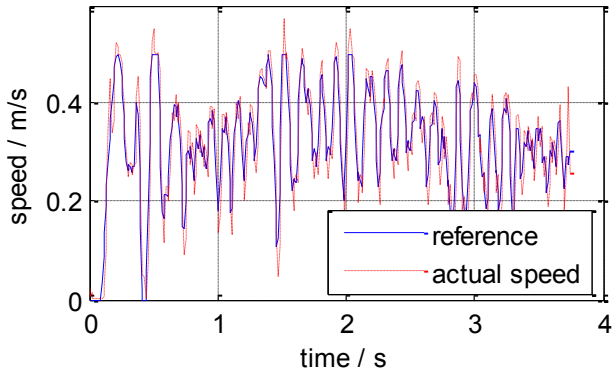

Fig-17 The time history of the speed of the end effector

The results in Fig-15 and 16 show that the speed control can also achieve the similar improvement of curing quality in face of the interference described in Fig-6. The speed profile in Fig-17 shows that the average sweeping speed of the end effector increases when it crosses the middle area of the target surface. Therefore, the corresponding irradiance decreases and counteracts the higher absorption of UV light.

According to the irradiance calculation equation (10), the irradiance distribution on the target surface is more sensitive to the relative geometric configuration than the radiant intensity. Therefore, the speed controller doesn't need to monitor the cured / uncured ratio h to adjust the shift speed. On the other hand, the radiant intensity controller has the advantage of achieving an even curing without any speed jerk. The two control strategies can be combined to solve more complicated problems in future study of the robotic UV curing process.

CONCLUSION

The contributions of this paper include the analysis of a robotic UV curing process and development of a closed-loop control approach by using thermal vision feedback through two IR cameras. A simple mathematical reduction of the model of the curing process is done to identify the primary state variables and control inputs. Two IR cameras are used to monitor the online temperature distribution of the target surface from both the local and global views. They are also integrated into the controller in a cascade manner. A simulation study is conducted to evaluate the proposed control strategy. Two cases are discussed, in which the radiant intensity and speed of the end effector are used as individual control variables under this thermal-vision-based architecture. The results show that the use of either control variable succeeds in compensating for interference and improving curing quality.

The future work may focus on developing a hybrid strategy combing both the radiant intensity and speed control in order to achieve an optimization of the robotic UV curing process. The authors are also developing an experimental system to demonstrate the proposed closed-loop control strategy for future industrial applications.

REFERENCES

[1] Schwalm, R., "UV Coatings: Basics, Recent Developments and New Applications," 1st ed. Amsterdam, Netherlands: Elsevier, 2007.

[2] Mills, P., "UV Curing for Automotive Exterior Applications: A cost-effective and technically viable alternative for UV curing," North American Automotive UV Consortium, Stongsville, OH, USA, 2005.

[3] Raith, T., Bischof, M., Deger, M., and Gemmler, E., "3-D UV Technology for OEM Coatings," RadTech Report Article on Robotic UV Curing at Daimler Chrysler, Germany, 2001.

[4] Zeng, F., Ayalew, B., and Omar, M., "Robotic Automotive Paint Curing Using Thermal Signature Feedback," *Industrial Robot: An International Journal,* 2008 (in press).

[5] Zeng, F., Ayalew, B., and Omar, M., "Cure-Feature Based Online Trajectory Generation in a Robotic Paint Curing System," *American Control Conference*, St. Louis, MO, USA, 2009 (in press).

[6] Hong, W., Lee, Y. T., and Gong, H., "Thermal Analysis of Layer formation in a Stepless Rapid Prototyping Process," *Applied Thermal Engineering,* vol. 24, pp. 255-268, February, 2004.

[7] Goodner, M. and Bowman, C., "Development of a Comprehensive Free Radical Photopolymerization Model Incorporating Heat and Mass Transfer Effects in Thick

Films," *Chemical Engineering Science,* vol. 57, pp. 887-900, March, 2002.
[8] Ashdown, I., "Radiosity: A Programmer's Perspective." New York, NY, USA: John Wiley & Sons, 1994.
[9] Modest, M., "Radiative Heat Transfer." New York, NY, USA: McGraw Hill, 1993.
[10] Paul, R., "Robot Manipulators: Mathematics, Programming, and Control." Cambridge, MA, USA: MIT Press, 1982.
[11] Sciavicco, L. and Siciliano, B., "Modeling and Control of Robot Manipulators." London, UK: Springer, 2000.